Shap. Mem. Superelasticity (2018) 4:85–92
https://doi.org/10.1007/s40830-018-0165-0

SPECIAL ISSUE: A TRIBUTE TO PROF. JAN VAN HUMBEECK – A LIFETIME OF CONTRIBUTIONS TO UNDERSTANDING MARTENSITE, INVITED PAPER

# H-Phase Precipitation and Martensitic Transformation in Ni-rich Ni–Ti–Hf and Ni–Ti-Zr High-Temperature Shape Memory Alloys

**A. Evirgen[1,2] · J. Pons[3] · I. Karaman[1] · R. Santamarta[3] · R. D. Noebe[4]**

Published online: 16 March 2018


**Abstract** The distributions of H-phase precipitates in $Ni_{50.3}Ti_{29.7}Hf_{20}$ and $Ni_{50.3}Ti_{29.7}Zr_{20}$ alloys formed by aging treatments at 500 and 550 °C or slow furnace cooling and their effects on the thermal martensitic transformation have been investigated by TEM and calorimetry. The comparative study clearly reveals faster precipitate-coarsening kinetics in the NiTiZr alloy than in NiTiHf. For precipitates of a similar size of 10–20 nm in both alloys, the martensite plates in $Ni_{50.3}Ti_{29.7}Zr_{20}$ have larger widths and span a higher number of precipitates compared with the $Ni_{50.3}Ti_{29.7}Hf_{20}$ alloy. However, for large H-phase particles with hundreds of nm in length, no significant differences in the martensitic microstructures of both alloy systems have been observed. The martensitic transformation temperatures of $Ni_{50.3}Ti_{29.7}Hf_{20}$ are ~ 80–90 °C higher than those of $Ni_{50.3}Ti_{29.7}Zr_{20}$ in the precipitate-free state and in the presence of large particles of hundreds on nm in length, but this difference is reduced to only 10–20 °C in samples with small H-phase precipitates. The changes in the transformation temperatures are consistent with the differences in the precipitate distributions between the two alloy systems observed by TEM.

✉ J. Pons
jaume.pons@uib.es

[1] Department of Materials Science and Engineering, A&M University, College Station, TX 77843, USA

[2] Present Address: Additive Manufacturing Division Oerlikon AM GmbH, D85622 Feldkirchen, Germany

[3] Departament de Fisica, Universitat de les Illes Balears, E07122 Palma De Mallorca, Spain

[4] Materials and Structures Division, NASA Glenn Research Center, Cleveland, OH 44135, USA

**Keywords** NiTiHf · NiTiZr · Aging · Transformation temperature · Precipitation

## Introduction

Ni–Ti shape memory alloys (SMAs) combine good mechanical and functional properties related to the thermoelastic martensitic transformation (MT) with excellent corrosion resistance, leading to the possibility of a large number of their applications in different industrial fields . However, new challenges in some of these industries (automotive, aerospace, energy exploration, …) demand a good actuating efficiency at elevated temperatures (> 100–150 °C), where binary NiTi SMAs cannot be used since their martensitic transformation temperatures lie below 100 °C [1]. Different macroalloying additions, such as Au, Pd, Pt, Hf, and Zr, have been found to increase the transformation temperatures (TTs) of the binary alloy [2]. Among these, NiTiPd and NiTiPt high-temperature shape memory alloys (HTSMAs) with high transformation temperatures and good thermal and dimensional stabilities have been developed in the last years [3–7]. The NiTiHf and NiTiZr systems have also been intensively studied as cheaper alternatives to the alloys containing precious metals. Most of the past studies on NiTiHf and NiTiZr HTSMAs were carried out on the (Ti+Hf/Zr)-rich compositions (above 50 at.%) since they exhibit higher transformation temperatures than the corresponding Ni-rich alloys [8–15]. However, these alloys present numerous disadvantages that prevented their commercial use, such as low recoverable and transformation strains, poor thermal and dimensional stability, and large hysteresis, caused by significant plasticity developed during the martensitic transformation as a result of the low strength of the alloys

at the actuating temperatures. Aging treatments tend to generate large $Ti_2Ni$-type particles in the (Ti+Hf/Zr)-rich compositions, but the large particles are not effective at strengthening the alloys, which is necessary for improving their shape memory response [8, 11].

It is well known that Ni-rich binary NiTi SMAs can be strengthened by suitable precipitation treatments generating nanosized $Ni_4Ti_3$ precipitates, which leads to excellent shape recovery and near-perfect dimensional stability [16–22]. These findings resulted in a shift in attention in the last decade toward Ni-rich NiTiHf and NiTiZr alloys. Early results were promising, and later work conclusively revealed that precipitation hardening is also an effective method to improve the shape memory response of Ni-rich NiTiHf/Zr SMAs. Early work by Meng and co-workers [23–25] already showed an improved thermal stability and shape recovery in NiTiHf alloys containing fine Ni-rich precipitates. Sandu et al. [26, 27] also observed nanosized precipitates in Ni-rich NiTiZr, which increased the hardness of the alloy. Later, completely recoverable strains up to $\sim 4\%$ in tension and $\sim -3\%$ in compression under 500 MPa at temperatures above 150 °C, as well as perfect superelasticity at 220 °C without any need of prior training were reported in a $Ni_{50.3}Ti_{29.7}Hf_{20}$ alloy containing 10–20 nm Ni-rich precipitates [28–31]. In the most recent years, the effects of different aging conditions on the functional properties of multiple Ni-rich Ni–Ti–Hf/Zr alloy compositions have been explored; see [32–43], and references therein].

The precipitated phase that effectively strengthens the Ni-rich Ni–Ti–Hf/Zr alloys is not the $Ni_4Ti_3$ phase, as occurs in Ni-rich binary NiTi alloys, but a new phase referred to simply as the "H-phase." Its crystal structure was initially studied by means of electron diffraction by Han et al. [44] and more recently by Yang et al. [45] and Santamarta et al. [46] using HRTEM imaging and DFT calculations for the structure refinement. The H-phase structure is built up as a superstructure of the B2 phase obtained from a recombination of the Hf/Zr and Ti atoms in their sublattice followed by a shuffling of all the atoms [45, 46]. The new phase is richer in Ni and ternary element content (Hf or Zr) and poorer in Ti in composition. There is a small lattice misfit between the H-phase and the B2 matrix, which allows for a full coherency and perfect lattice plane matching at the austenite/precipitate interface over distances larger than 50 nm [46].

In previous work, Evirgen et al. developed a systematic investigation of thermal treatments to generate a variety of distributions of H-phase precipitates in Ni-rich NiTiHf and NiTiZr alloys containing 15 at.% and 20 at.% Hf/Zr and studied their effects on the MT and functional properties [32–34]. Dense distributions of fine precipitates of a few tens of nm in size were found to improve the functional properties (shape memory effect and superelasticity), resulting in recoverable actuation strains up to 4% at 170 °C and superelasticity at 250 °C up to 3% applied strain with good dimensional stability and a very small amount of unrecovered strain attributed to precipitation hardening. The fine precipitates also reduced the transformation hysteresis in relation to the solution heat-treated alloys with no precipitates, which showed larger amounts of irrecoverable strains. In turn, samples with dispersed H-phase particles of hundreds of nanometers in length presented more fragility and significantly lower recoverable actuation strains and larger hysteresis compared with the materials with nanometric precipitates [32–34]. Moreover, small precipitate size and interparticle spacing generated by low-temperature aging treatments (450–500 °C) for short durations produced a decrease of the MTTs compared with the precipitate-free state. This was ascribed to the strain energy developed around the closely spaced unsheared precipitates during the MT of the surrounding matrix. In turn, larger precipitate volume fractions, induced by longer aging at low temperatures or aging at elevated temperatures, produce a significant increase of the MTTs, attributed to larger precipitate size with much greater interparticle distance and greater Ni depletion of the transforming matrix caused by the H-phase precipitation [33, 34].

The two alloy systems, Ni-rich NiTiHf and NiTiZr, exhibit a parallel behavior in the sense that the same H-phase (with equivalent crystal structure) precipitates in both alloys [46] and they present similar general effects of the precipitates on the MTTs and functional properties [33, 34]. However, to our knowledge, a systematic comparative behavior of both alloy systems is lacking in the literature and, thus, constitutes the main purpose of the present work. Several H-phase precipitation treatments, e.g., aging at 500 and 550 °C or slow furnace-cooling treatments, are studied in alloys with the same stoichiometry: $Ni_{50.3}Ti_{29.7}Hf_{20}$ and $Ni_{50.3}Ti_{29.7}Zr_{20}$. The precipitate distributions formed in both alloys under equivalent treatments are compared, together with their effects on the thermal martensitic transformation.

## Materials and Methods

Alloys with the nominal compositions $Ni_{50.3}Ti_{29.7}Hf_{20}$ and $Ni_{50.3}Ti_{29.7}Zr_{20}$ (at.%) were induction melted in a graphite crucible under inert Argon atmosphere using high-purity elemental materials (99.98% Ni, 99.95% Ti, 99.9% Hf, 99.9% Zr). The ingots were homogenized at 1050 °C for 72 h and sealed in mild steel cans, followed by hot extrusion at 900 °C with an area reduction ratio of 7:1. Samples were electrical discharge machined from the extruded rods

and sealed in quartz tubes under protective argon atmosphere. Subsequently, they were solution heat treated (SHT) at 900 °C for 1 h and water quenched to provide a homogeneous structure. Disperse carbide particles (mostly HfC or ZrC) of micrometric size were also present in the microstructure [33, 34], arising from the reaction of the melt with the graphite crucible during vacuum.

Induction melting of the alloys. Based on our previous studies [32–34], several precipitation heat treatments were chosen to be applied on the SHT specimens to obtain two-phase microstructures with different precipitate sizes, which increase the transformation temperatures in relation to the precipitate-free materials and result in different martensite morphologies. A first group of specimens were aged at 500 °C for 3 h or 48 h and at 550 °C for 3 h followed by water quenching to generate dispersions of H-phase precipitates of a few tens of nm in size. Another group of samples were held at 700 °C for 5 min and furnace cooled (FC) to 100 °C in 3 or 48 h and water quenched to produce large H-phase particles of hundreds of nm in size. Finally, a third group of samples were investigated in the SHT state as a reference material without any precipitates. Hereafter, the different thermally processed samples of $Ni_{50.3}Ti_{29.7}Hf_{20}$ (labeled as NTH) and $Ni_{50.3}Ti_{29.7}Zr_{20}$ (labeled as NTZ) will be coded to indicate their compositions and heat-treatment conditions. For instance, NTZ5003 and NTZFC48 correspond to the $Ni_{50.3}Ti_{29.7}Zr_{20}$ samples that were aged at 500 °C for 3 h, and furnace cooled from 700 to 100 °C in 48 h, respectively. All the samples were sealed in quartz tubes under argon atmosphere to prevent oxidation during heat treatments and water quenched by breaking the quartz tubes.

DSC experiments were performed in TA Instruments Q20e calorimeter at a heating/cooling rate of 10 K/min. TEM observations at room temperature were performed in JEOL 2011 high-resolution microscope (phase contrast mode) with $LaB_6$ filament, operated at 200 kV. Specimens for TEM investigations were prepared by double-jet electrochemical polishing using a 30% $HNO_3$ and 70% ethanol solution at around 20 °C and ~ 12 V.

## Results and Discussion

Figure 1a–h shows brightfield TEM images to compare the precipitate size and morphology in $Ni_{50.3}Ti_{29.7}Zr_{20}$ (right-hand-side images) and $Ni_{50.3}Ti_{29.7}Hf_{20}$ (left-hand-side images) for the different precipitation treatments. The precipitate morphology is the same in both alloys: spindle like in shape when they are nanometric sized (Fig. 1a–f) and prolate ellipsoids or plate like in shape similar to martensite variants when they reach several hundred nanometers in size (Fig. 1g–h). The precipitate sizes resulting from all heat treatments are summarized in Table 1. In all cases, the $Ni_{50.3}Ti_{29.7}Zr_{20}$ samples contain significantly larger precipitates compared with $Ni_{50.3}Ti_{29.7}Hf_{20}$ samples under the same heat-treatment condition. Therefore, based on the present TEM observations, it can be concluded that the precipitate-coarsening kinetics are faster in the NiTiZr alloy than that in the NiTiHf alloy for the same relative stoichiometry. For instance, after 3 h at 500 °C, the precipitates in NiTiZr grow to 10–25 nm in length (Fig. 1b), whereas 48-h aging at the same

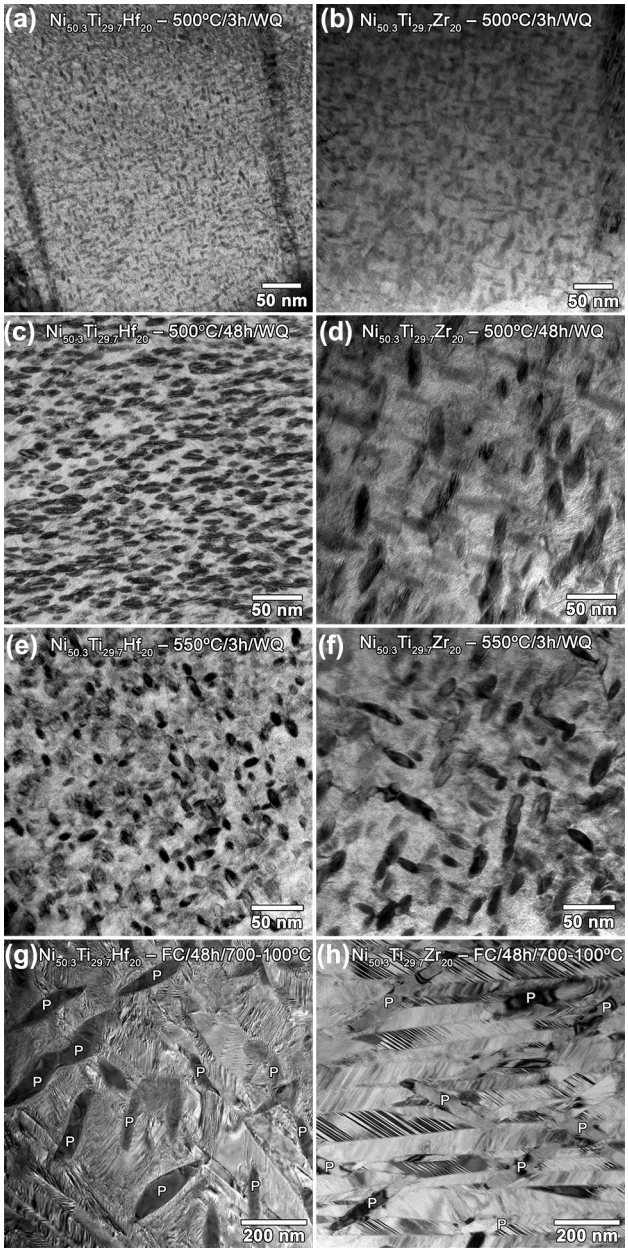


**Fig. 1** Brightfield TEM images of Ni50.3Ti29.7Hf20 (left) and Ni50.3Ti29.7Zr20 (right) samples aged at 500 °C for 3 h **a** and **b**; aged at 500 °C for 48 h **c** and **d**; aged at 550 °C for 3 h **e** and **f** and furnace cooled from 700 to 100 °C in 48 h **g** and **h**

temperature are needed to produce similar size in NiTiHf (Fig. 1c). The same trend holds for the further coarsening of the precipitates, since in NiTiZr it takes only 3 h of furnace cooling from 700 to 100 °C for the precipitate sizes to reach several hundreds of nanometers, while the precipitates in the NiTiHf reach similar size after 48 h of furnace cooling.

In agreement with previous work [46], Fig. 1 shows that the small precipitates are completely embedded in the martensite variants, which span a large number of precipitates. In contrast, the large particles formed after furnace cooling (> 100 nm) are impenetrable obstacles that limit the martensite growth within the spaces between precipitates, leading to martensite variants with comparable sizes to those of the precipitates (Fig. 1g). Since the precipitate size is shown to have a strong effect on the martensite morphology, it is also important to study the martensite plate thickness in both alloys. For this purpose, Fig. 2a, b presents low-magnification images of NTZ5003 and NTH50048 samples which, according to Table 1, have similar precipitate sizes. Comparing Fig. 2a, b, it becomes clear that the martensite plate thickness in the NiTiZr alloy is much larger than that in the NiTiHf alloy for similar precipitate sizes. This observation is evidence for an easier accommodation of the transformation strain around the precipitates in NiTiZr alloys than that in NiTiHf, as already pointed out in our previous work and attributed to lower values of transformation strain and stiffness of the austenite and H-phase in the NiTiZr alloys [46].

For the furnace-cooled samples with large H-phase particles, the precipitate sizes are similar in the NTZFC3 and NTHFC48 samples (Table 1). From the TEM images of these samples (Fig. 2c, d), no obvious difference can be detected in the martensite plate size of both alloys. In this type of microstructure, the martensite variants can grow only within the space left in between the precipitates and, therefore, their sizes are mostly dependent on the interparticle distances. For the NTZFC3 and NTHFC48 samples, the TEM images do not differ remarkably in both alloys.

The DSC thermograms registered for all the specimens are shown in Fig. 3, and Table 2 summarizes the values of the martensite start, *M*s, and austenite finish, *Af*, temperatures, thermal hysteresis, $\Delta T$ (calculated as $\Delta T = Af - Ms$) and difference between the *M*s values in the first and third cycles ($Ms_1 - Ms_3$) for both systems. In both alloys, the transformation temperatures increase with the precipitation treatments due to the Ni-depletion of the matrix. Furthermore, for the aging treatments at 500 and 550 °C, producing nanometric precipitates, the thermal hysteresis decreases in comparison with the SHT material as a consequence of precipitation hardening. In turn, the thermal hysteresis increases significantly for the furnace-cooled samples, where a large density of tiny martensite variants are generated, limited by the large precipitate obstacles, and therefore, energy dissipation is increased. In addition, the thermal stability of the alloy improves when precipitates are present, as already reported in [35]. The shifts in *M*s temperature after 2 or 3 consecutive cycles are reduced due to a lower defect generation during the martensitic transformation caused by precipitation hardening in the aged and furnace-cooled samples, compared with the SHT material. Such general behaviors of the present NiTiZr and NiTiHf alloys are equivalent to that reported previously for the NiTiZr and NiTiHf alloys with 15 at.% content in Hf/Zr [33, 34].

Comparing the transformation temperatures and transformation characteristics of both alloys, for the SHT (precipitate-free) state (see Table 2), the $Ni_{50.3}Ti_{29.7}Hf_{20}$ alloy shows much higher transformation temperatures than those of $Ni_{50.3}Ti_{29.7}Zr_{20}$, which indicates that the Hf addition to NiTi is more effective than Zr for increasing the transformation temperatures, in agreement with previous studies [2]. However, in the materials submitted to nanometric precipitation treatments (aging at 500 or 550 °C), the data in Table 2 indicate that the *M*s temperatures are

**Table 1** Approximate precipitate sizes of $Ni_{50.3}Ti_{29.7}Zr_{20}$ and $Ni_{50.3}Ti_{29.7}Hf_{20}$ alloys for different thermal treatments

| Alloy | Treatment | Label | Precipitate size (nm) | |
|---|---|---|---|---|
| | | | Length | Width |
| $Ni_{50.3}Ti_{29.7}Zr_{20}$ | 3 h @ 500 °C | NTZ5003 | 10–25 | 5–11 |
| | 48 h @ 500 °C | NTZ50048 | 20–40 | 10–15 |
| | 3 h @ 550 °C | NTZ5503 | 18–45 | 7–14 |
| | FC 700–100 °C 48 h | NTZFC48 | 200–500 | 35–55 |
| | FC 700–100 °C 3 h | NTZFC3 | 90–280 | 25–45 |
| $Ni_{50.3}Ti_{29.7}Hf_{20}$ | 3 h @ 500 °C | NTH5003 | 6–8 | 2–4 |
| | 48 h @ 500 °C | NTH50048 | 8–20 | 3–8 |
| | 3 h @ 550 °C | NTH5503 | 7–20 | 4–6 |
| | FC 700–100 °C 48 h | NTHFC48 | 70–250 | 20–70 |

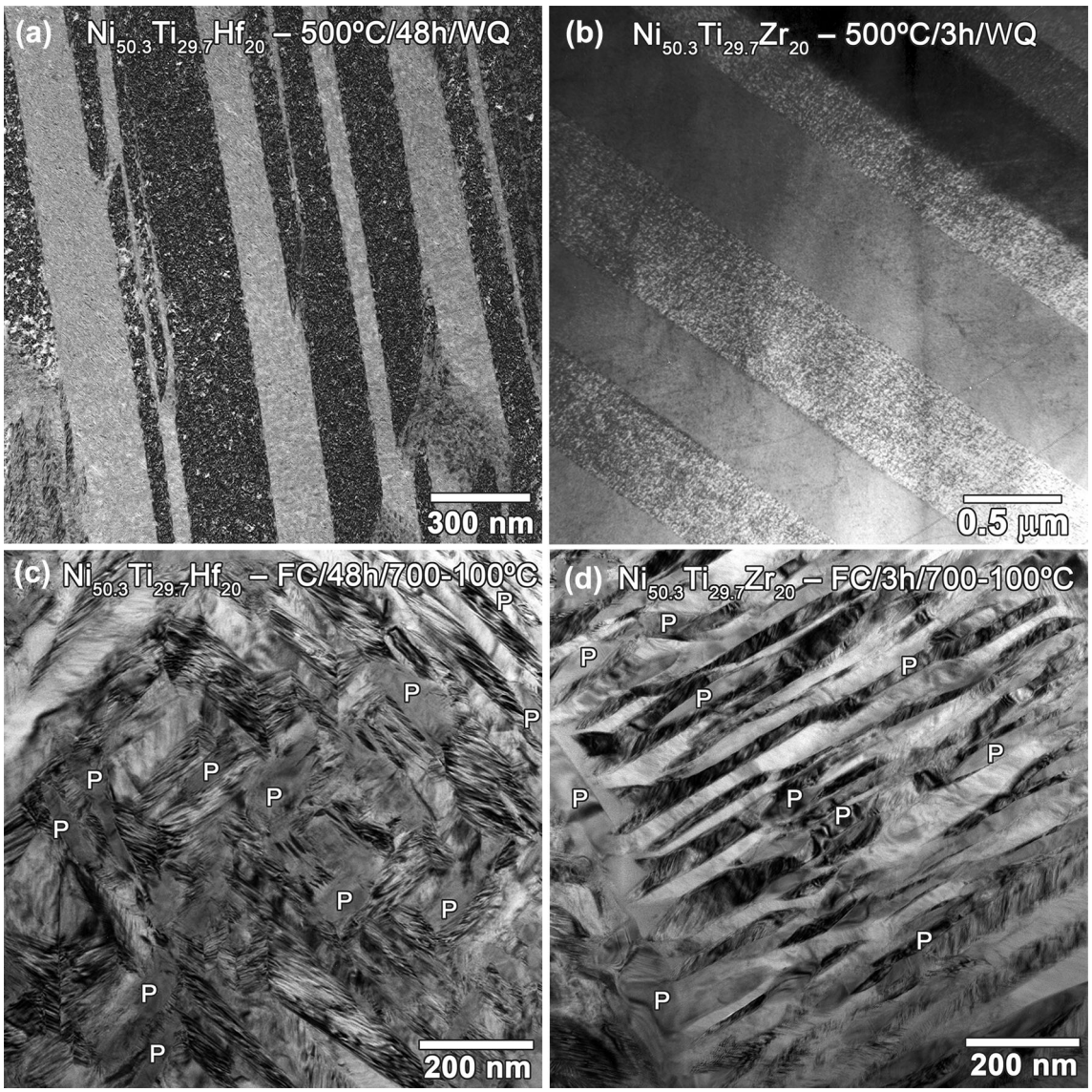


**Fig. 2** Brightfield TEM images of samples with similar precipitate sizes. **a** Ni50.3Ti29.7Hf20 aged at 550 °C for 3 h; **b** Ni50.3Ti29.7Zr20 aged at 500 °C for 3 h); **c** Ni50.3Ti29.7Hf20 furnace cooled from 700 to 100 °C in 48 h and **d** Ni50.3Ti29.7Zr20 furnace cooled from 700 to 100 °C in 3 h

only 10–20 °C higher in the $Ni_{50.3}Ti_{29.7}Hf_{20}$ alloy compared with $Ni_{50.3}Ti_{29.7}Zr_{20}$, and the *Af* temperatures are nearly the same for both alloys. For the furnace-cooled samples containing large particles, the transformation temperatures are again much higher in $Ni_{50.3}Ti_{29.7}Hf_{20}$.

The thermal hysteresis ($\Delta T$) values are significantly smaller in the $Ni_{50.3}Ti_{29.7}Hf_{20}$ alloy (38 °C) compared with $Ni_{50.3}Ti_{29.7}Zr_{20}$ (68 °C) in precipitate-free conditions (SHT). When nanometric precipitates are present, the thermal hysteresis in $Ni_{50.3}Ti_{29.7}Zr_{20}$ is only 10–20 °C higher than the corresponding $Ni_{50.3}Ti_{29.7}Hf_{20}$ alloys. On the other hand, $\Delta T$ values get closer in both systems when the precipitates are hundreds of nanometers in size, after furnace cooling. The shift in *Ms* temperatures ($Ms_1$–$Ms_3$), which is a measure of thermal stability, is also smaller in the $Ni_{50.3}Ti_{29.7}Hf_{20}$ alloy compared with the $Ni_{50.3}Ti_{29.7}Zr_{20}$ alloy when there are no precipitates or when the precipitates are nanometric in size, indicating that the $Ni_{50.3}Ti_{29.7}Hf_{20}$ alloy is more stable. In fact, in a previous work [47], we showed that the B2 phase of $Ni_{50.3}Ti_{29.7}Zr_{20}$ is unstable at low temperatures (around 250 °C) and undergoes short-range atomic-reordering processes that tend to decrease the MTTs. As a consequence, the shift in the *Ms* temperature upon thermal cycling was shown to increase when the upper cycle temperature in the DSC experiments was raised [47]. In the present work, the $Ni_{50.3}Ti_{29.7}Zr_{20}$ samples were cycled in the DSC up to 300 °C (see Fig. 3), which contributes to the large $Ms_1$–$Ms_3$ values obtained

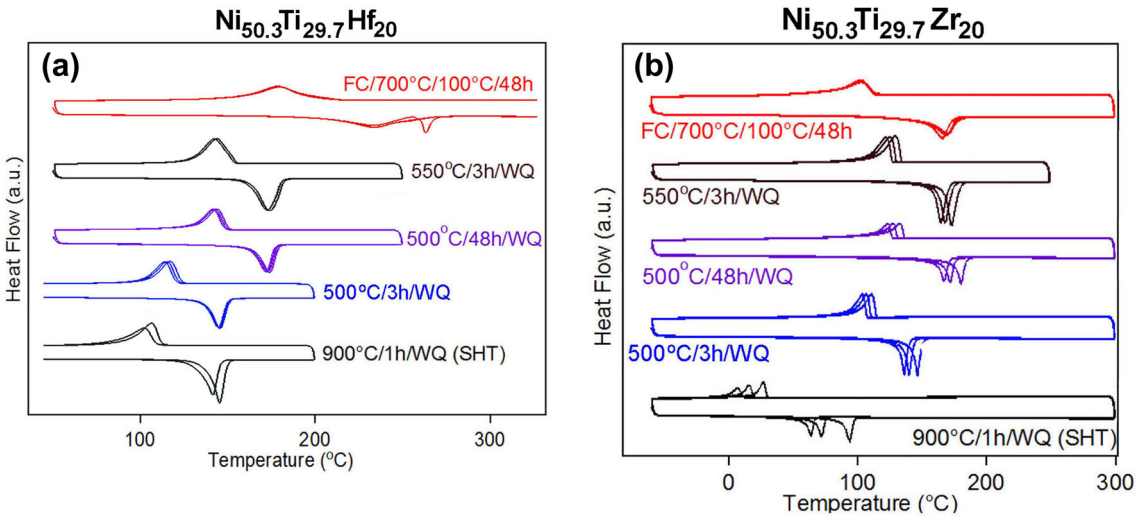


**Fig. 3** DSC thermograms registered from Ni50.3Ti29.7Hf20 **a** and Ni50.3Ti29.7Zr20 **b** alloys after various precipitation treatments

**Table 2** Values of austenite finish, *Af*, and martensite start, *M*s, temperatures, thermal hysteresis calculated as $T = Af - Ms$, and change in *M*s temperatures for the first three cycles ($Ms_1$–$Ms_3$) obtained from the DSC thermograms of $Ni_{50.3}Ti_{29.7}Zr_{20}$ and $Ni_{50.3}Ti_{29.7}Hf_{20}$ under various thermal treatment conditions

| Alloy | Treatment | *Af* (°C) | *M*s (°C) | *T* (°C) | $Ms_1$–$Ms_3$ (°C) |
|---|---|---|---|---|---|
| $Ni_{50.3}Ti_{29.7}Zr_{20}$ | SHT | 98 | 30 | 68 | 19 |
| | 3 h @ 500 °C | 151 | 114 | 37 | 7 |
| | 48 h @ 500 °C | 185 | 136 | 49 | 9 |
| | 3 h @ 550 °C | 180 | 134 | 46 | 7 |
| | FC 700–100 °C 48 h | 175 | 113 | 62 | − 2 |
| $Ni_{50.3}Ti_{29.7}Hf_{20}$ | SHT | 150 | 112 | 38 | 3.3 (2 cycles) |
| | 3 h @ 500 °C | 151 | 123 | 27 | 3.2 |
| | 48 h @ 500 °C | 179 | 150 | 29 | 2.3 |
| | 3 h @ 550 °C | 182 | 155 | 27 | 1.5 (2 cycles) |
| | FC 700–100 °C 48 h | 268 | 202 | 66 | 1 |

(Table 2). In turn, the furnace cooling treatments producing large precipitates leave the alloys in a state closer to equilibrium. As a consequence, the thermal reproducibility is improved and becomes very similar for both alloys, with very little change in *M*s temperatures with thermal cycling.

The transformation temperatures in the alloys containing H-phase precipitates are mostly affected by two different mechanisms: a mechanical effect related to the strain energy needed to accommodate the transformation strain of the matrix around the nontransforming precipitates, which tends to decrease the *M*s temperature, and a compositional effect related to Ni depletion of the matrix by the Ni-rich H-phase particles, which tends to increase the transformation temperatures [33, 34]. The present TEM images of Fig. 2 demonstrate an easier accommodation of the small precipitates with the martensite in the $Ni_{50.3}Ti_{29.7}Zr_{20}$ alloy compared with the $Ni_{50.3}Ti_{29.7}Hf_{20}$ after aging at 500 or 550 °C, which would tend to produce a smaller decrease in the *M*s temperature for the former alloy. At the same time, the Ni depletion of the matrix is assumed to be higher in the $Ni_{50.3}Ti_{29.7}Zr_{20}$ alloy, as the precipitates attain larger sizes than that in $Ni_{50.3}Ti_{29.7}Hf_{20}$ for the same treatments, as shown in Table 1. Therefore, from the TEM observations, it can be deduced that the small precipitates absorbed by the martensite plates should produce a larger increase of the transformation temperatures in $Ni_{50.3}Ti_{29.7}Zr_{20}$ than in $Ni_{50.3}Ti_{29.7}Hf_{20}$, in good agreement with the DSC observations (Table 2). For such precipitate distributions, the large difference in *M*s values of both alloys in the precipitate-free state is largely reduced by the differences in the precipitate size and accommodation with martensite. On the other hand, for the furnace-cooled material with large particles, the Ni depletion of the transforming matrix is the dominant effect. As seen in Figs. 1 g and h, the volume fraction of H-phase is similar in both alloys furnace cooled for 48 h, for which it can be assumed that the precipitates produce similar effects on the transformation. Therefore, the transformation temperatures of the $Ni_{50.3}Ti_{29.7}Hf_{20}$ furnace-cooled samples are again much larger than those of

$Ni_{50.3}Ti_{29.7}Zr_{20}$ due to the greater intrinsic effect of Hf addition on TT.

## Conclusions

The present work focused on the comparison of H-phase precipitate distributions formed in $Ni_{50.3}Ti_{29.7}Hf_{20}$ and $Ni_{50.3}Ti_{29.7}Zr_{20}$ alloys under various precipitation treatments, and their effects on the martensitic transformation characteristics. The main conclusions are the following:

- For each of the precipitation treatments investigated, the H-phase precipitates attain larger sizes in the $Ni_{50.3}Ti_{29.7}Zr_{20}$ alloy than those in $Ni_{50.3}Ti_{29.7}Hf_{20}$. Therefore, the precipitate-coarsening kinetics are faster in the NiTiZr alloy than those in NiTiHf for the same relative stoichiometry.
- Comparing samples with similar precipitate size of a few tens of nanometers in both alloys, the martensite plates attain notably larger widths and span a higher number of precipitates in $Ni_{50.3}Ti_{29.7}Zr_{20}$ than those in $Ni_{50.3}Ti_{29.7}Hf_{20}$. This better accommodation of precipitates within the martensite phase for the Zr containing alloy completely confirms our previous observations [46]. However, for large H-phase particles with hundreds of nanometers in length which act as impenetrable obstacles for the martensite plates, the TEM images do not reveal significant differences in the martensitic microstructures of both alloy systems.
- The martensitic transformation temperatures are $\sim 80$ °C higher in $Ni_{50.3}Ti_{29.7}Hf_{20}$ than those in $Ni_{50.3}Ti_{29.7}Zr_{20}$ in the precipitate-free state, confirming that the Hf addition is more effective than Zr addition for increasing the transformation temperatures of the binary NiTi alloys. However, in samples containing small H-phase precipitates, the difference is largely reduced, and the transformation temperatures are only 10–20 °C higher in the Hf-containing alloy. In turn, for samples with large particles of hundreds on nanometers in length, the transformation temperatures are again much larger in $Ni_{50.3}Ti_{29.7}Hf_{20}$ than those in $Ni_{50.3}Ti_{29.7}Zr_{20}$. The changes in the transformation temperatures are consistent with the differences in the precipitate distributions between the two alloy systems observed by TEM, and confirm the mechanisms based on the mechanical effect related to the strain energy developed in the matrix around the nontransforming precipitates and the compositional effect related to the Ni depletion of the matrix.
- For samples containing precipitates of few tens of nanometers, the thermal hystereses of both $Ni_{50.3}Ti_{29.7}Hf_{20}$ and $Ni_{50.3}Ti_{29.7}Zr_{20}$ decrease in comparison with the SHT material as a consequence of precipitation hardening, being 10–20 °C larger in $Ni_{50.3}Ti_{29.7}Zr_{20}$ than in $Ni_{50.3}Ti_{29.7}Hf_{20}$. Instead, for large particles of hundreds of nanometers in length, the hysteresis is largely increased due to the drastic change of the martensitic microstructure.

**Acknowledgements** Partial financial support from the Spanish MINECO and FEDER under project number MAT2014-56116-C4-1-R is gratefully acknowledged. RDN gratefully acknowledges support from the NASA Transformative Aeronautics Concepts Program, Transformational Tools & Technologies Project, and Othmane Benafan, Technical Lead for Shape Memory Alloy Development.

## References

1. Otsuka K, Ren X (2005) Physical metallurgy of Ti–Ni-based shape memory alloys. Prog Mater Sci 50:511–678
2. Ma J, Karaman I, Noebe RD (2010) High temperature shape memory alloys. Int Mater Rev 55:257–315
3. Bigelow GS, Padula SA II, Garg A, Gaydosh D, Noebe RD (2010) Characterization of ternary NiTiPd high-temperature shape-memory alloys under load-biased thermal cycling. Met Mat Trans A 41A:3065–3079
4. Kockar B, Atli KC, Ma J, Haouaoui M, Karaman I, Nagasako M, Kainuma R (2010) Role of severe plastic deformation on the cyclic reversibility of a Ti50.3Ni33.7Pd16 high temperature shape memory alloy. Acta Mater 58:6411–6420
5. Atli KC, Karaman I, Noebe RD, Garg A, Chumlyakov YI, Kireeva IV (2011) Shape memory characteristics of Ti49.5Ni25Pd25Sc0.5 high-temperature shape memory alloy after severe plastic deformation. Acta Mater 59:4747–4760
6. Monroe JA, Karaman I, Lagoudas DC, Bigelow G, Noebe RD, Padula S II (2011) Determining recoverable and irrecoverable contributions to accumulated strain in a NiTiPd high-temperature shape memory alloy during thermomechanical cycling. Scr Mater 65:123–126
7. Khan MI, Kim HY, Namigata Y, Nam T, Miyazaki S (2013) Combined effects of work hardening and precipitation strengthening on the cyclic stability of TiNiPdCu-based high-temperature shape memory alloys. Acta Mater 61:4797–4810
8. Olier P, Brachet JC, Bechade JL, Foucher C, Guenin G (1995) Investigation of transformation temperatures, microstructure and shape memory properties of NiTi, NiTiZr and NiTiHf alloys. J Phys IV C8:741–746
9. Angst DR, Thoma PE, Kao MY (1995) The effect of Hf content on the transformation temperatures of Ni49Ti51-xHfx shape memory alloys. J Phys IV C8:747–752
10. Besseghini S, Villa E, Tuissi A (1999) Ni-Ti-Hf shape memory alloy: effect of aging and thermal cycling. Mat Sci Eng A 273:390–394
11. Wu SK, Hsieh SF (2000) Martensitic transformation of a Ti-rich Ti40.5Ni49.5Zr10 shape memory alloy. J Alloy Comp 297:294–302
12. Meng X, Zheng Y, Cai W, Zhao L (2004) Two-way shape memory effect of a TiNiHf high temperature shape memory alloy. J Alloy Compd 372:180–186
13. Firstov GS, Van Humbeeck J, Koval YN (2004) Comparison of high temperature shape memory behaviour for ZrCu-based, Ti–Ni–Zr and Ti–Ni–Hf alloys. Scripta Mater 50:243–248

14. Kockar B, Karaman I, Kim JI, Chumlyakov YI (2006) A method to enhance cyclic reversibility of NiTiHf high temperature shape memory alloys. Scripta Mater 54:2203–2208
15. Kim HY, Mizutani M, Miyazaki S (2009) Crystallization process and shape memory properties of Ti–Ni–Zr thin films. Acta Mater 57:1920–1930
16. Nishida M, Wayman CM, Honma T (1986) Precipitation processes in near-equiatomic TiNi shape memory alloys. Met Trans 17:1505–1515
17. Gall K, Sehitoglu H, Chumlyakov YI, Zuev YL, Karaman I (1998) The role of coherent precipitates in martensitic transformations in single crystal and polycrystalline Ti-50.8at%Ni. Scripta Mater 39:699–705
18. Sehitoglu H, Jun J, Zhang XY, Karaman I, Chumlyakov YI, Maier HJ, Gall K (2001) Shape memory and pseudoelastic behavior of 51.5%Ni–Ti single crystals in solutionized and overaged state. Acta Mater 49:3609–3620
19. Khalil-Allafi J, Dlouhy A, Eggeler G (2002) Ni4Ti3-precipitation during aging of NiTi shape memory alloys and its influence on martensitic phase transformations. Acta Mater 50:4255–4274
20. Chumlyakov YI, Panchenko EY, Aksenov VB, Kireeva IV, Kuksa MP, Karaman I, Sehitoglu H (2004) The shape memory effect and superelasticity in Ti-Ni single crystals with one variant of dispersed particles. J Phys IV 115:21–28
21. Kim JI, Miyazaki S (2005) Effect of nano-scaled precipitates on shape memory behavior of Ti-50.9at.%Ni alloy. Acta Mater 53:4545–4554
22. Panchenko E, Chumlyakov YI, Kireeva I, Ovsyannikov A, Sehitoglu H, Karaman I, Maier HJ (2008) Effect of disperse Ti3Ni4 particles on the martensitic transformations in titanium nickelide single crystals. Phys Metall Metall 106:577–589
23. Meng X, Cai W, Zheng Y, Zhao LC (2006) Phase transformation and precipitation in aged Ti–Ni–Hf high-temperature shape memory alloys. Mat. Sci. Eng. A 438–440:666–670
24. Meng X, Cai W, Chen F, Zhao LC (2006) Effect of aging on martensitic transformation and microstructure in Ni-rich TiNiHf shape memory alloy. Scripta Mater 54:1599–1604
25. Meng X, Cai W, Fu YD, Li QF, Zhang JX, Zhao LC (2008) Shape-memory behaviors in an aged Ni-rich TiNiHf high temperature shape-memory alloy. Intermetallics 16:698–705
26. Sandu AM, Tsuchiya K, Yamamoto S, Todaka Y, Umemoto M (2006) Influence of isothermal ageing on mechanical behaviour in Ni-rich Ti–Zr–Ni shape memory alloy. Scripta Mater 55:1079–1082
27. Sandu AM, Tsuchiya K, Tabuchi M, Yamamoto S, Todaka Y, Umemoto M (2007) Microstructural evolution during isothermal aging in Ni-Rich Ti-Zr-Ni shape memory alloys. Mater Trans 48:432–438
28. Bigelow GS, Garg A, Padula li SA, Gaydosh DJ, Noebe RD (2011) Load-biased shape-memory and superelastic properties of a precipitation strengthened high-temperature Ni50.3Ti29.7Hf20 alloy. Scripta Mater 64:725–728
29. Coughlin DR, Phillips PJ, Bigelow GS, Garg A, Noebe RD, Mills MJ (2012) Characterization of the microstructure and mechanical properties of a 50.3Ni–29.7Ti–20Hf shape memory alloy. Scripta Mater 67:112–115
30. Benafan O, Noebe RD, Padula SA II, Vaidyanathan R (2012) Microstructural response during isothermal and isobaric loading of a precipitation-strengthened Ni-29.7Ti-20Hf high-temperature shape memory alloy. Metall Mater Trans A 43:4539–4552
31. Karaca HE, Saghaian SM, Basaran B, Bigelow GS, Noebe RD, Chumlyakov YI (2011) Compressive response of nickel-rich NiTiHf high-temperature shape memory single crystals along the [1 1 1] orientation. Scripta Mater 65:577–580
32. Evirgen A, Karaman I, Santamarta R, Pons J, Noebe RD (2014) Microstructural characterization and superelastic response of a Ni50.3Ti29.7Zr20 high temperature shape memory alloy. Scripta Mater 81:12–15
33. Evirgen A, Karaman I, Santamarta R, Pons J, Noebe RD (2015) Microstructural characterization and shape memory characteristics of the Ni50.3Ti34.7Hf15 shape memory alloy. Acta Mater 83:48–60
34. Evirgen A, Karaman I, Pons J, Santamarta R, Noebe RD (2016) Role of nano-precipitation on the microstructure and shape memory characteristics of a new Ni50.3Ti34.7Zr15 shape memory alloy. Mat Sci Eng A 655:193–203
35. Karaca HE, Saghaian SM, Ded G, Tobe H, Basaran B, Maier HJ, Noebe RD, Chumlyakov YI (2013) Effects of nanoprecipitation on the shape memory and material properties of an Ni-rich NiTiHf high temperature shape memory alloy. Acta Mat. 61:7422–7431
36. Saghaian SM, Karaca HE, Tobe H, Souri M, Noebe RD, Chumlyakov YI (2015) Effects of aging on the shape memory behavior of Ni-rich Ni50.3Ti29.7Hf20 single crystals. Acta Mater 87:128–141
37. Saghaian SM, Karaca HE, Souri M, Turabi AS, Noebe RD (2016) Tensile shape memory behavior of Ni50.3Ti29.7Hf20 high temperature shape memory alloys. Mat Design 101:340–345
38. Benafan O, Garg A, Noebe RD, Bigelow GS, Padula SA II, Gaydosh DJ, Schell N, Mabe JH, Vaidyanathan R (2014) Mechanical and functional behavior of a Ni-rich Ni50.3Ti29.7Hf20 high temperature shape memory alloy. Intermetallics 50:94–107
39. Stebner AP, Bigelow GS, Yang J, Shukla DP, Saghaian SM, Rogers R, Garg A, Karaca HE, Chumlyakov Y, Bhattacharya K, Noebe RD (2014) Transformation strains and temperatures of a nickel–titanium–hafnium high temperature shape memory alloy. Acta Mater 76:40–53
40. Atli KC, Karaman I, Noebe RD, Bigelow G, Gaydosh D (2015) Work production using the two-way shape memory effect in NiTi and a Ni-rich NiTiHf high-temperature shape memory alloy. Smart Mater Struct 24:125023
41. Patriarca L, Sehitoglu H, Panchenko Y, Chumlyakov YI (2016) High-temperature functional behavior of single crystal Ni51.2Ti23.4Hf25.4 shape memory alloy. Acta Mater 106:333–343
42. Sehitoglu H, Patriarca L, Wu Y (2017) Shape memory strains and temperatures in the extreme. Curr Opin Solid State Mater Sci 21:113–120
43. Karakoc O, Hayrettin C, Bass M, Wang SJ, Canadinc D, Mabe JH, Lagoudas DC, Karaman I (2017) Effects of upper cycle temperature on the actuation fatigue response of NiTiHf high temperature shape memory alloys. Acta Mater 138:185–197
44. Han XD, Wang R, Zhang Z, Yang DZ (1998) A new precipitate phase in a TiNiHf high temperature shape memory alloy. Acta Mater 46:273–281
45. Yang F, Coughlin DR, Phillips PJ, Yang L, Devaraj A, Kovarik L, Noebe RD, Mills MJ (2013) Structure analysis of a precipitate phase in an Ni-rich high-temperature NiTiHf shape memory alloy. Acta Mater 61:3335–3346
46. Santamarta R, Arroyave R, Pons J, Evirgen A, Karaman I, Karaca HE, Noebe RD (2013) TEM study of structural and microstructural characteristics of a precipitate phase in Ni-rich Ni-Ti-Hf and Ni-Ti-Zr shape memory alloys. Acta Mater 61:6191–6206
47. Pérez-Sierra AM, Pons J, Santamarta R, Karaman I, Noebe RD (2016) Stability of a Ni-rich Ni-Ti-Zr high temperature shape-memory alloy upon low temperature aging and thermal cycling. Scripta Mater 124:47–50